

Spatially-resolved dielectric constant of confined water and its connection to the non-local nature of bulk water

Christian Schaaf^{1,2} and Stephan Gekle²

¹*Institute of Theoretical Physics, Technical University Berlin, Hardenbergstraße 36, 10623 Berlin, Germany*

²*Biofluid Simulation and Modeling, Fachbereich Physik, Universität Bayreuth, Universitätsstraße 30, Bayreuth 95440, Germany*

(Dated: August 24, 2016)

We use Molecular Dynamics simulations to compute the spatially resolved static dielectric constant of water in cylindrical and spherical nanopores as occurring, e.g., in protein water pockets or carbon nanotubes. For this, we derive a linear-response formalism which correctly takes into account the dielectric boundary conditions in the considered geometries. We find that in cylindrical confinement the axial component behaves similar as the local density akin to what is known near planar interfaces. The radial dielectric constant shows some oscillatory features when approaching the surface if their radius is larger than about 2nm. Most importantly, however, the radial component exhibits pronounced oscillations at the center of the cavity. These surprising features are traced back quantitatively to the non-local dielectric nature of bulk water.

Published as: J. Chem. Phys. **145**, 084901 (2016), doi:10.1063/1.4960775

I. INTRODUCTION

The behavior of water's hydrogen bond network under nanometric confinement has become a very active and important research field in chemical physics¹⁻⁹. Such situations occur naturally, e.g., for water in protein pockets or aquaporins¹⁰ but also in technological applications such as the construction of filter membranes and pumping systems using carbon nanotubes or pores¹¹⁻¹³. In many of these situations, water is directly affected by electric fields originating either from close-by charges, such as in proteins, from internal charges, such as in salt solutions, or from external fields. It thus seems essential to gain detailed knowledge how water locally reacts to these fields. For this, the central question is if and how the dielectric constant of confined water is (or is not) different from bulk water.

In confinement, or near interfaces in general, the dielectric constant ϵ is no longer a simple number, but depends on the position relative to the interface and in addition becomes tensorial. A lot of work has been invested recently in attempts to understand this anisotropic spatially dependent dielectric constant for various geometries mainly using Molecular Dynamics (MD) simulations. The dielectric water properties¹⁴⁻¹⁷ have been investigated near rigid planar interfaces¹⁸⁻²⁷, soft interfaces²⁸⁻³², aqueous solutions³³⁻⁴³ or around spherical solutes⁴⁴. As a general trend, the spatially resolved dielectric constant becomes oscillatory reminiscent of the well-known density oscillations in interfacial water. Experimentally, current techniques are mainly based on spectroscopy and thus far only allow a spatially averaged determination of the dielectric properties in the interfacial region⁴⁵⁻⁵⁶

The dielectric constant of water in non-planar confinements, however, has received less attention. Under spherical confinement Refs. 57 and 58 defined an effective, isotropic dielectric constant which was found to be

reduced compared to the bulk fluid. In addition, Ref. 59 investigated the radial component of the anisotropic permittivity tensor far away from both the center and the confining wall. For the important case of cylindrical confinement such as in carbon nanotubes or aquaporins, the axial component has recently been found to be roughly (though not exactly) proportional to the local density^{60,61}. For the radial component which will be most relevant for solvated ions, the only currently existing works did not employ the appropriate fluctuation equation casting doubts on some of their results⁶²⁻⁶⁷.

Here we use Molecular Dynamics (MD) simulations to compute the spatially resolved static dielectric constant in axial and radial directions for cylindrical nanopores as well as the radial component in spherical nanocavities. The profile of the axial dielectric constant in cylindrical confinement exhibits a very similar shape as the density profile which is reminiscent of a planar wall^{22,24} in agreement with refs. 60,61. For the radial dielectric constant, the influence of the wall can only be distinguished for relatively large tubes with radii above 2nm. However, strong oscillations are found at the *center* for cylindrical and spherical confinement. This is surprising as water in this region would a priori be expected to be bulk-like. Indeed, we show that these oscillations are fully explainable if one considers the full non-local nature of bulk water. Only for very small tubes or spheres with radii of the order of 0.5nm the dielectric properties of water near the center truly deviate from bulk water. We expect that these oscillations in the radial dielectric constant will have profound implications for the solvation energy of ions in tubes or pores.

The remainder of the paper is organized as follows. In section II we briefly introduce the Molecular Dynamics simulation method. In section III we derive the required linear-response equations as well as the non-local formalism. Section IV presents our results and section V contains concluding remarks.

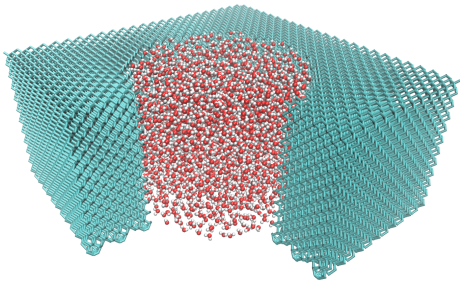


Figure 1. Snapshot of the cylindrical system. The cyan grid illustrates the carbon atoms.

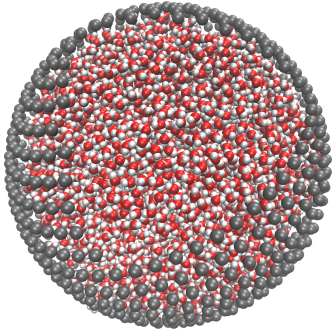


Figure 2. Snapshot of the spherical system. The black particles enclose water molecules to ensure spherical symmetry over the simulation time.

II. METHODS

We conduct classical MD simulations using Gromacs⁶⁸ and the SPC/E water model⁶⁹. In this model the oxygen has the Lennard-Jones parameters $\sigma_{OO} = 0.31656\text{nm}$ and $\epsilon_{OO} = 0.65017\text{kJ/mol}$ and the charge $q_O = -0.8476e$. Hydrogen atoms possess no Lennard-Jones interactions but do have a positive charge of $q_H = -0.5q_O$. For the van-der-Waals potential we use a cutoff radius of 1 nm (switched after 0.9 nm). The time step is 2 fs and electrostatics are calculated using the usual particle-mesh Ewald summation.

The cylindrical cavities are carved out of a cubic lattice of carbon atoms by simply removing all C atoms within the cavity as illustrated in figure 1. The carbon atoms are then frozen during the simulation and have the Lennard-Jones interaction parameters of $\sigma_{CO} = 0.33670\text{nm}$ and $\epsilon_{CO} = 0.42469\text{kJ/mol}$. We study four cylindrical pores with radii $r_c = 0.5\text{nm}$, 1.0nm , 2.0nm and 2.5nm . The total system size is $8.5 \times 8.5 \times 4\text{ nm}$ for the 2.5nm pore and $9 \times 9 \times 5\text{ nm}$ for the other three. In order to determine the amount of water molecules within the tube we first fill the entire box with randomly arranged water molecules at bulk density. We then remove all water molecules whose oxygen is located at a radial position larger than $r_c - r_{\text{shift}}$ where r_{shift} is introduced to avoid direct overlap with the wall. We usually choose $r_{\text{shift}} = 0.2\text{nm}$. We have checked that varying the amount of water molecules in a range $\pm 5\%$ does not significantly influence the results.

For the spherical system we use the same setup as in Ref. 44 without the solute in the center of the sphere as can be seen in figure 2. A droplet of water molecules is enclosed by a layer of frozen uncharged wall particles with Lennard-Jones interactions parameters $\sigma_{eO} = 0.25\text{nm}$ and $\epsilon_{eO} = 0.62\text{kJ/mol}$. These wall particles ensure the spherical symmetry over the whole simulation time. The three employed sphere radii are $R_s = 0.7\text{nm}$, 1.0nm and 2.0nm and the amount of contained water is determined in the same manner as for the cylinder above.

The number of water molecules as well as the simulation time for both systems are listed in tables I and II.

r_c [nm]	#H ₂ O	simulation time [ns]
0.5	52	120
1.0	341	80
2.0	1708	2200
2.5	2518	5800

Table I. Number of water molecules and simulation time for the cylindrical setup. The simulation time for the two larger pores has to be that long to reduce the noise in the interfacial region.

R_s [nm]	#H ₂ O	simulation time [ns]
0.7	47	200
1.0	144	200
2.0	1116	360

Table II. Number of water molecules and simulation time for the spherical setup.

III. THEORY

A. Linear response formalism in confined water

In order to derive a linear response (or fluctuation) equation for the dielectric constant, we consider an electric field in direction α of a geometry-adapted coordinate system in which the dielectric tensor is diagonal. For the cylindrical geometry α can be radial (denoted r) or axial (denoted z) while for the spherical cavity we only consider the radial (denoted R) direction. In both geometries there further exists a tangential component which is not investigated in the present work.

We start by considering the cylindrical geometry in which all quantities only depend on r and the definition of the local dielectric constant $\epsilon_\alpha(r)$ is

$$\Delta P_\alpha(r) = (\epsilon_\alpha(r) - 1) \epsilon_0 \Delta E_\alpha^{\text{int}}(r) \quad (1)$$

where ΔP_α denotes the change in the local polarization caused by a change of the internal, or Maxwell, field $\Delta E_\alpha^{\text{int}}$ and ϵ_0 is the vacuum permittivity. Microscopically, the phase space average of the polarization when

an external field is present is written as

$$\langle P_\alpha(r) \rangle_E = \frac{\int d\Omega P_\alpha(r) e^{-\beta(H+W_\alpha)}}{\int d\Omega e^{-\beta(H+W_\alpha)}} \quad (2)$$

where H is the Hamiltonian of the system in the field-free case, and $\beta = 1/(k_B T)$ with the Boltzmann constant k_B and the temperature T . Furthermore, W_α is the additional energy due to the interaction with the electric field. This interaction energy is given by

$$W_\alpha = - \int_V P_\alpha(r) E_\alpha^{\text{ext}}(r) dV \quad (3)$$

where $E_\alpha^{\text{ext}}(r)$ denotes the external field which in general can be different from the internal (Maxwell) field. In order to obtain a fluctuation formula one requires an explicit relation between the internal and external fields. This relation depends on the considered geometry and on the direction α . From now on the two directions need to be treated separately. For the axial direction the field is parallel to all dielectric boundaries and thus

$$E_z^{\text{int}}(r) = E_z^{\text{ext}}(r). \quad (4)$$

At the same time the external field is independent of r and the interaction energy reads

$$\begin{aligned} W_z &= -E_z^{\text{ext}} \int_V P_z(r) dV \\ &= -E_z^{\text{ext}} 2\pi L \int_0^{r_c} r P_z(r) dr \end{aligned} \quad (5)$$

with the cylinder length L and the cylinder radius r_c . Linearizing Eq. (2) for small E_z^{ext} gives

$$\begin{aligned} \langle P_z(r) \rangle_E &\approx \langle P_z(r) \rangle_0 - \beta E_z^{\text{ext}} \left(\left\langle P_z(r) \frac{\partial W_z}{\partial E_z^{\text{ext}}} \right\rangle_0 \right. \\ &\quad \left. - \langle P_z(r) \rangle_0 \left\langle \frac{\partial W_z}{\partial E_z^{\text{ext}}} \right\rangle_0 \right) \end{aligned} \quad (6)$$

where $\langle \dots \rangle_0$ denotes a phase space average in the absence of the external field. Using

$$\Delta P_\alpha(r) = \langle P_\alpha(r) \rangle_E - \langle P_\alpha(r) \rangle_0 \quad (7)$$

one then equates Eq. (1) and Eq. (6) and eliminates E^{ext} by Eq. (4) to obtain

$$\begin{aligned} \varepsilon_z(r) &= 1 + \frac{\beta 2\pi L}{\varepsilon_0} \left(\left\langle P_z(r) \int_0^{r_c} r' P_z(r') dr' \right\rangle_0 \right. \\ &\quad \left. - \langle P_z(r) \rangle_0 \left\langle \int_0^{r_c} r' P_z(r') dr' \right\rangle_0 \right). \end{aligned} \quad (8)$$

The axial polarization $P_z(r)$ is calculated from the MD simulations using the local dipole density since higher order multipoles have been found to be negligible for the wall-parallel dielectric component²².

For the radial direction we consider the field emanating from a line charge q/L at the center. This field is perpendicular to the dielectric boundaries leading to

$$\begin{aligned} E_r^{\text{ext}}(r) &= \frac{1}{2\pi\varepsilon_0} \frac{q}{rL} \\ &= E_r^{\text{int}}(r) \varepsilon_r(r). \end{aligned} \quad (9)$$

The corresponding interaction energy reads

$$\begin{aligned} W_r &= - \int_V P_r(r) E_r^{\text{ext}}(r) dV \\ &= - \int_V P_r(r) \frac{1}{2\pi\varepsilon_0} \frac{q}{Lr} dV \\ &= - \frac{q}{\varepsilon_0} \int_0^{r_c} P_r(r) dr \end{aligned} \quad (10)$$

Using Eq. (10) in Eq. (2), linearizing with respect to small q and equating with Eq. (1), one obtains the correct fluctuation equation for the radial dielectric constant in cylindrical geometry⁶⁵

$$\begin{aligned} \frac{\varepsilon_r(r) - 1}{\varepsilon_r(r)} &= \frac{2\pi\beta r L}{\varepsilon_0} \left(\left\langle P_r(r) \int_0^{r_c} P_r(r') dr' \right\rangle_0 \right. \\ &\quad \left. - \langle P_r(r) \rangle_0 \left\langle \int_0^{r_c} P_r(r') dr' \right\rangle_0 \right) \end{aligned} \quad (11)$$

We note that erroneously assuming equality of the internal and external radial fields as has been done in several earlier publications^{62–64,66,67} would lead to an equation of the form

$$\begin{aligned} \varepsilon_r^*(r) &= 1 + \frac{\beta 2\pi L}{\varepsilon_0} \left(\left\langle P_r(r) \int_0^{r_c} r' P_r(r') dr' \right\rangle_0 \right. \\ &\quad \left. - \langle P_r(r) \rangle_0 \left\langle \int_0^{r_c} r' P_r(r') dr' \right\rangle_0 \right). \end{aligned} \quad (12)$$

Such fluctuation formulas have no physical basis and therefore do not lead to correct results.

For the spherical geometry the procedure is completely analogous, except that one considers a point charge instead of a line charge. The final result is

$$\begin{aligned} \frac{\varepsilon_R(R) - 1}{\varepsilon_R(R)} &= \frac{4\pi\beta R^2}{\varepsilon_0} \left(\left\langle P_R(R) \int_0^{R_s} P_R(R') dR' \right\rangle_0 \right. \\ &\quad \left. - \langle P_R(R) \rangle_0 \left\langle \int_0^{R_s} P_R(R') dR' \right\rangle_0 \right) \end{aligned} \quad (13)$$

in agreement with the equation derived earlier by⁵⁹.

B. Non-local formalism

In a bulk medium with non-local dielectric properties such as water, the polarization \vec{P} at any point \vec{r} can be written as

$$\vec{P}(\vec{r}) = \varepsilon_0 \int_V (\varepsilon_{\text{nl}}(\vec{r}, \vec{r}') - \delta(\vec{r} - \vec{r}')) \vec{E}(\vec{r}') d\vec{r}' \quad (14)$$

where the integral extends over all space. In a homogeneous medium, the non-local dielectric constant depends only on the distance between the source and the observation point⁷⁰ and can thus be written as:

$$\varepsilon_{\text{nl}}(\vec{r}, \vec{r}') = \varepsilon_{\text{nl}}(|\vec{r} - \vec{r}'|). \quad (15)$$

Due to translational invariance the non-local dielectric constant is conveniently treated in Fourier space $\varepsilon_{\text{nl}}(k)$ where it can be obtained from MD simulations of bulk water. In the following we use the data from our earlier work⁴⁴ which is similar to the data of Bopp et al.^{71,72}

We proceed to compute the internal electric potential for a field emanating radially from a line or a point in a non-local dielectric bulk medium. This allows us to relate the non-local formalism to the locally observed ε_r and ε_R which can be computed from MD simulations as described in the previous paragraph. While it is possible to treat non-local electrostatics also in finite media^{73,74}, one of our goals here is to show that the radial response in a non-local bulk medium can be quantitatively related to the local response caused by an appropriate electric field geometry. Therefore we do not attempt to apply the non-local formalism directly to the confined situation.

Consider a uniformly charged hollow cylinder with radius a , length L and total charge q . The charge density on the cylinder mantle is then

$$\rho(r) = \frac{q}{2\pi aL} \delta(r - a). \quad (16)$$

The Fourier transform of an axially symmetric and z -independent function $f(r)$ is⁷⁵

$$f(\vec{k}) = \int_0^\infty dr 4\pi^2 r f(r) J_0(k_r r) \delta(k_z) \quad (17)$$

where J_0 is the zeroth-order Bessel function. Using Eq. (17) on Eq. (16) gives

$$\rho(\vec{k}) = \frac{2\pi q}{L} J_0(k_r a) \delta(k_z). \quad (18)$$

Now the cylinder is placed into water with the non-local dielectric constant in wave-vector space given as $\varepsilon_{\text{nl}}(k)$. In order to compute the internal potential $\phi^{\text{int}}(r)$, we need to solve the non-local Poisson equation^{70,73,76}

$$\rho(\vec{r}) = -\varepsilon_0 \nabla \cdot \int_V \varepsilon_{\text{nl}}(\vec{r} - \vec{r}') \nabla \phi^{\text{int}}(\vec{r}') d\vec{r}'. \quad (19)$$

In Fourier space, this becomes

$$\varepsilon_0 k^2 \varepsilon_{\text{nl}}(k) \phi^{\text{int}}(\vec{k}) = \rho(\vec{k}) \quad (20)$$

leading to

$$\phi^{\text{int}}(\vec{k}) = \frac{1}{\varepsilon_0 k^2} \frac{1}{\varepsilon_{\text{nl}}(k)} \rho(\vec{k}). \quad (21)$$

The inverse Fourier transform back to real space is simplified by using $\varphi = 0$ without loss of generality

$$\begin{aligned} \phi^{\text{int}}(r) &= \frac{1}{(2\pi)^3} \int_0^\infty dk_r k_r \int_0^{2\pi} dk_\varphi \int_{-\infty}^\infty dk_z \phi^{\text{int}}(\vec{k}) \times \\ &\times e^{ik_r r \cos(k_\varphi)} e^{ik_z z} \end{aligned} \quad (22)$$

Using Eq. (18) in Eq. (21) and substituting in Eq. (22) gives

$$\phi^{\text{int}}(r) = \int_0^\infty \frac{1}{\varepsilon_{\text{nl}}(k_r)} \frac{q}{2\pi \varepsilon_0 k_r L} J_0(k_r r) J_0(k_r a) dk_r. \quad (23)$$

Now take the limit $a \rightarrow 0$ for a line charge at the center and compute the internal field

$$\begin{aligned} E_r^{\text{int}}(r) &= -\nabla \phi^{\text{int}}(r) \\ &= \frac{q}{2\pi \varepsilon_0 L} \int_0^\infty dk_r \frac{1}{\varepsilon_{\text{nl}}(k_r)} J_1(k_r r). \end{aligned} \quad (24)$$

Finally, we use Eq. (9) with Eq. (24) to find

$$\begin{aligned} \varepsilon_r^{-1}(r) &= \frac{E_r^{\text{int}}(r)}{E_r^{\text{ext}}(r)} \\ &= \int_0^\infty \frac{1}{\varepsilon_{\text{nl}}(k_r)} r J_1(k_r r) dk_r \end{aligned} \quad (25)$$

which represents a direct relation between the local dielectric constant obtained from MD simulations under confinement and the non-local dielectric constant of bulk water.

For a point charge, an analogous derivation in spherical coordinates leads to

$$\varepsilon_R^{-1}(R) = \frac{2}{\pi} R^2 \int_0^\infty \frac{1}{\varepsilon_{\text{nl}}(k)} \left(\frac{\sin(kR)}{kR^2} - \frac{\cos(kR)}{R} \right) dk \quad (26)$$

IV. RESULTS

Figure 1 shows an illustration of the employed system to investigate the dielectric constant in cylindrical confinement. The local water density $\rho_m(r)$ is plotted in Fig. 3 (a). Due to symmetry any quantity in this system only depends on the radial position r . For the two larger pores with $r_c=2.5\text{nm}$ and $r_c=2\text{nm}$ we observe pronounced density oscillations up to roughly 1nm away from the surface. Beyond that distance the density attains its constant bulk value. The density oscillations are similar to those observed near planar hydrophobic interfaces²⁴. For the two smaller pores the density oscillations range up to and including the central axis such that a bulk regime is not observed.

The axial component of the dielectric tensor $\varepsilon_z(r)$ computed from the fluctuation equation (8) is shown in figure 3 (b). Here, the bulk regime with $\varepsilon_z = 71$ for SPC/E water⁷⁷ is attained roughly 0.5nm away from the surface. The oscillations in $\varepsilon_z(r)$ are similar to those in the mass density $\rho_m(r)$ with the same wave length and similar amplitudes. The only exception is the first peak which is somewhat higher in $\varepsilon_z(r)$ than in $\rho_m(r)$. This behavior is similar to the one observed near a planar interface²² and in agreement with other recent works in cylindrical confinement^{60,61}.

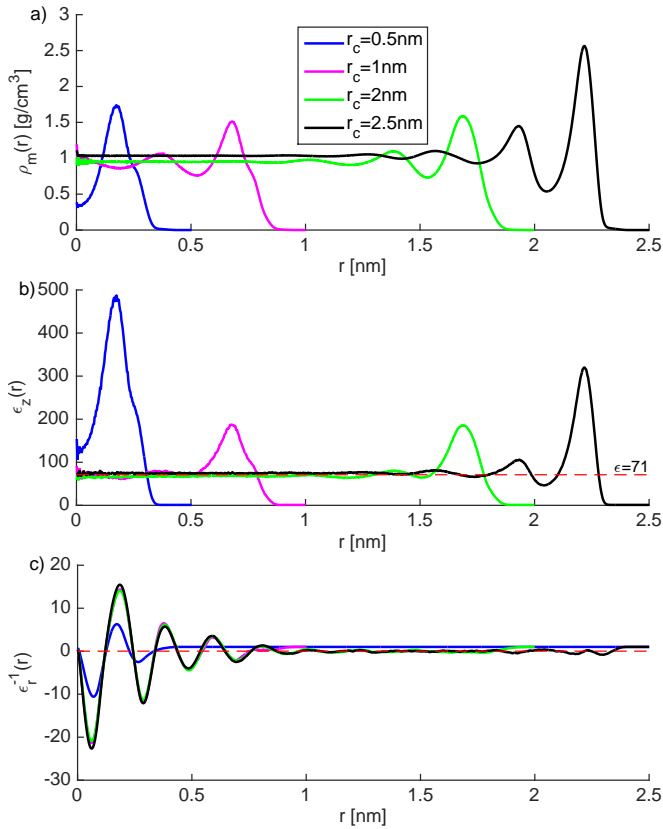


Figure 3. (a) Density profile for the four considered cylindrical nanopores. (b)+(c) Profiles of the spatially resolved axial (b) and radial (c) dielectric constant. While the axial component is almost proportional to the local density, the radial component exhibits pronounced oscillations near the central axis which are investigated further in Figure 4 below.

Figure 3 (c) shows the inverse of the radial dielectric constant as calculated from the fluctuation equation (11). The most prominent feature here are the strong oscillations around the center of the tube. At first sight, these might seem to be an artifact of the simulation. However, as will be shown below, they possess a clear physical origin which can be traced back to the non-local nature of the dielectric constant in bulk water.

Another interesting observation is that only weak changes to the radial dielectric constant are observed near the pore wall. This can be appreciated by the closer view in figure 4 (a). For the 2.5nm pore some weak and rather noisy oscillations are seen which are reminiscent of those observed earlier near a planar wall^{22,24}. The oscillations become noticeably weaker for the 2nm pore indicating that the higher curvature of the interface allows the water to cover this curved wall more smoothly and with less disruptions of the hydrogen bond network. For the two smallest pores the near-wall features are obscured by the dominant features of non-local origin, cf. figure 3 (c).

Figure 4 (b) shows a close-up of the inverse radial component around the central axis of the four investigated tubes. With the exception of the smallest tube

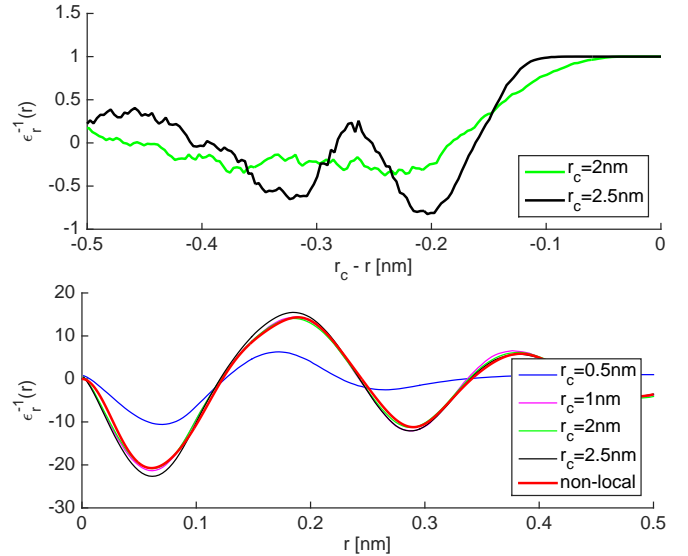


Figure 4. (a) Close-up view of the radial dielectric constant near the walls of cylindrical pores from figure 3 (c). Only for the largest pore with $r_c = 2.5\text{nm}$ significant oscillations analogous to the ones observed near a planar wall are seen. (b) Close-up view of the radial dielectric constant near the center of the cylindrical pores from figure 3 (c). Except for the smallest pore with $r_c = 0.5\text{nm}$, all profiles show the same behavior which is in quantitative agreement with a prediction derived from the non-local properties of bulk water in Eq. (25).

with $r_c = 0.5\text{nm}$, all curves overlap. This already indicates that the origin of these oscillations might be related to properties of bulk water and not to an interaction with the confining wall. Indeed, the prediction for $\varepsilon_r(r)$ from Eq. (25) which is based purely on bulk properties fits the observed profiles extremely well (red curve). These results illustrate that a spatially varying dielectric constant observed under confinement is not necessarily connected to a change in (interfacial) water properties, but may simply be a direct consequence of the non-local characteristics of bulk water. The agreement between direct MD and the non-local prediction disappears only for cylindrical cavities whose radius is smaller than 1nm as shown by the blue profile for $r_c = 0.5\text{nm}$. This observation indicates an important transition. For small cavities all contained water must be considered "interfacial" with properties differing from bulk, while in cavities with $r_c \geq 1\text{nm}$ the water around the central axis is already bulk-like.

In order to bring out the general nature of this conclusion, we extend our investigations to water in spherical confinement. Figure 5 shows the spatially resolved radial component of the dielectric tensor $\varepsilon_R(R)$ as obtained from the fluctuation equation (13). Again, very good agreement with the non-local bulk prediction of Eq. (26) is observed for cavities with radii $R_s \geq 1\text{nm}$. For smaller cavities, the agreement disappears due to an increased disruption of the hydrogen bond network in so strongly

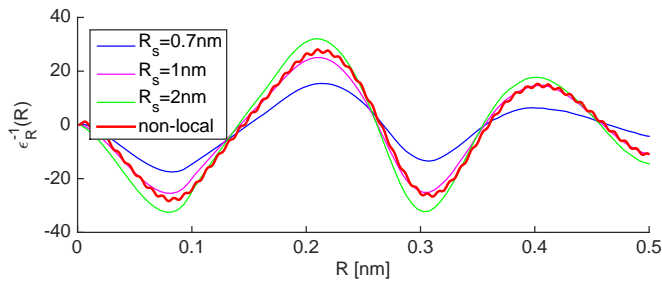


Figure 5. (a) The radial dielectric constant of water in spherical confinement. Near the center, the oscillations are again in agreement with a non-local bulk water prediction from Eq. (26).

confined water.

V. CONCLUSION

Using Molecular Dynamics simulations we have computed the radial and axial components of the spatially resolved dielectric tensor of water in cylindrical and spherical confinement. The investigated pores are of a generic hydrophobic nature mimicking water confined in carbon nanotubes or hydrophobic protein pockets. The axial component near the walls of cylindrical pores scales roughly with the local density, an effect that has also been observed in the vicinity of planar interfaces.

Our most important finding is that the radial component features pronounced oscillations near the center of the cylindrical or spherical confinement. These oscillations are traced back to the non-local nature of bulk water in combination with the radial field geometry. They are independent of the confinement itself as long as the pore radius is not smaller than about 1 nm.

The radial dielectric component is essential for the free energy of solvated ions in water. We thus expect that our observations may have important applications in the study of membrane systems as used for desalination or ion channels through cell membranes.

ACKNOWLEDGMENTS

The authors gratefully acknowledge funding from the Volkswagen Foundation as well as computing time granted by the John von Neumann Institute for Computing (NIC) and provided on the supercomputer JURECA at Jülich Supercomputing Centre (JSC).

REFERENCES

¹M. Sega, R. Vallauri, and S. Melchionna, “Diffusion of water in confined geometry: The case of a multilamellar bilayer,” *Phys. Rev. E* **72**, 041201–4 (2005).

²H.-S. Tan, I. R. Piletic, and M. D. Fayer, “Orientational dynamics of water confined on a nanometer length scale in reverse micelles,” *J. Chem. Phys.* **122**, 174501 (2005).

³J. C. Rasaiah, S. Garde, and G. Hummer, “Water in Nonpolar Confinement: From Nanotubes to Proteins and Beyond,” *Annu. Rev. Phys. Chem.* **59**, 713–740 (2008).

⁴W. Pezeshkian, N. Nikoofard, D. Norouzi, F. Mohammad-Rafiee, and H. Fazli, “Distribution of counterions and interaction between two similarly charged dielectric slabs: Roles of charge discreteness and dielectric inhomogeneity,” *Phys. Rev. E* **85**, 061925 (2012).

⁵A. A. Bakulin, D. Cringus, P. A. Pieniazek, J. L. Skinner, T. L. C. Jansen, and M. S. Pshenichnikov, “Dynamics of Water Confined in Reversed Micelles: Multidimensional Vibrational Spectroscopy Study,” *J. Phys. Chem. B* **117**, 15545–15558 (2013).

⁶B. Kim, S. Kwon, H. Mun, S. An, and W. Jhe, “Energy dissipation of nanoconfined hydration layer: Long-range hydration on the hydrophilic solid surface,” *Sci. Rep.* **4**, 6499 (2014).

⁷M. F. Harrach, F. Klameth, B. Drossel, and M. Vogel, “Effect of the hydroaffinity and topology of pore walls on the structure and dynamics of confined water,” *J. Chem. Phys.* **142**, 034703–8 (2015).

⁸M. Jahn and S. Gekle, “Bulk and interfacial liquid water as a transient network,” *Phys. Rev. E* **92**, 052130–10 (2015).

⁹S. Cerveny, F. Mallamace, J. Swenson, M. Vogel, and L. Xu, “Confined Water as Model of Supercooled Water,” *Chem. Rev.* (2016).

¹⁰P. Ball, “Water as an Active Constituent in Cell Biology,” *Chem. Rev.* **108**, 74–108 (2008).

¹¹S. Porada, B. B. Sales, H. V. M. Hamelers, and P. M. Biesheuvel, “Water Desalination with Wires,” *J. Phys. Chem. Lett.* **3**, 1613–1618 (2012).

¹²K. F. Rinne, S. Gekle, D. J. Bonthuis, and R. R. Netz, “Nanoscale Pumping of Water by AC Electric Fields,” *Nano Lett.* **12**, 1780–1783 (2012).

¹³D. Cohen-Tanugi and J. C. Grossman, “Mechanical Strength of Nanoporous Graphene as a Desalination Membrane,” *Nano Lett.* **14**, 6171–6178 (2014).

¹⁴D. Pan, L. Spanu, B. Harrison, D. A. Sverjensky, and G. Galli, “Dielectric properties of water under extreme conditions and transport of carbonates in the deep Earth,” *Proc. Nat. Acad. Sci. (USA)* **110**, 6646–6650 (2013).

¹⁵L. Shi, Y. Ni, S. E. P. Drews, and J. L. Skinner, “Dielectric constant and low-frequency infrared spectra for liquid water and ice Ih within the E3B model,” *J. Chem. Phys.* **141**, 084508–10 (2014).

¹⁶C. Zhang and G. Galli, “Dipolar correlations in liquid water,” *J. Chem. Phys.* **141**, 084504–5 (2014).

¹⁷M. Sega and C. Schröder, “Dielectric and Terahertz Spectroscopy of Polarizable and Nonpolarizable Water Models: A Comparative Study,” *J. Phys. Chem. A* **119**, 1539–1547 (2015).

¹⁸J. Martí, G. Nagy, E. Guàrdia, and M. C. Gordillo, “Molecular Dynamics Simulation of Liquid Water Confined inside Graphite Channels: Dielectric and Dynamical Properties,” *J. Phys. Chem. B* **110**, 23987–23994 (2006).

¹⁹V. A. Froltsov and S. H. L. Klapp, “Anisotropic dynamics of dipolar liquids in narrow slit pores,” *J. Chem. Phys.* **124**, 134701 (2006).

²⁰V. A. Froltsov and S. H. L. Klapp, “Dielectric response of polar liquids in narrow slit pores,” *J. Chem. Phys.* **126**, 114703 (2007).

²¹M. C. F. Wander and A. E. Clark, “Structural and Dielectric Properties of Quartz-Water Interfaces,” *J. Phys. Chem. C* **112**, 19986–19994 (2008).

²²D. J. Bonthuis, S. Gekle, and R. R. Netz, “Dielectric Profile of Interfacial Water and its Effect on Double-Layer Capacitance,” *Phys. Rev. Lett.* **107**, 166102 (2011).

²³D. J. Bonthuis, S. Gekle, and R. R. Netz, “Profile of the Static Permittivity Tensor of Water at Interfaces: Consequences for Capacitance, Hydration Interaction and Ion Adsorption,” *Langmuir* **28**, 7679–7694 (2012).

- ²⁴S. Gekle and R. R. Netz, "Anisotropy in the Dielectric Spectrum of Hydration Water and its Relation to Water Dynamics," *J. Chem. Phys.* **137**, 104704 (2012).
- ²⁵C. Zhang, F. Gygi, and G. Galli, "Strongly Anisotropic Dielectric Relaxation of Water at the Nanoscale," *J. Phys. Chem. Lett.* **4**, 2477–2481 (2013).
- ²⁶S. Parez, M. Předota, and M. Machesky, "Dielectric Properties of Water at Rutile and Graphite Surfaces: Effect of Molecular Structure," *J. Phys. Chem. C* **118**, 4818–4834 (2014).
- ²⁷H. Itoh and H. Sakuma, "Dielectric constant of water as a function of separation in a slab geometry: A molecular dynamics study," *J. Chem. Phys.* **142**, 184703–10 (2015).
- ²⁸H. A. Stern and S. E. Feller, "Calculation of the Dielectric Permittivity Profile for a Nonuniform System: Application to a Lipid Bilayer Simulation," *J. Chem. Phys.* **118**, 3401 (2003).
- ²⁹S. Pal, S. Balasubramanian, and B. Bagchi, "Anomalous dielectric relaxation of water molecules at the surface of an aqueous micelle," *J. Chem. Phys.* **120**, 1912 (2004).
- ³⁰M. Ahmad, W. Gu, T. Geyer, and V. Helms, "Adhesive water networks facilitate binding of protein interfaces," *Nature Communications* **2**, 261 (2011).
- ³¹W. C. Guest, N. R. Cashman, and S. S. Plotkin, "A theory for the anisotropic and inhomogeneous dielectric properties of proteins," *Phys. Chem. Chem. Phys.* **13**, 6286 (2011).
- ³²S. Gekle and R. R. Netz, "Nanometer-Resolved Radio-Frequency Absorption and Heating in Biomembrane Hydration Layers," *J. Phys. Chem. B* **118**, 4963–4969 (2014).
- ³³A. Chandra, "Static dielectric constant of aqueous electrolyte solutions: Is there any dynamic contribution?" *J. Chem. Phys.* **113**, 903 (2000).
- ³⁴S. Boresch, M. Willensdorfer, and O. Steinhauser, "A molecular dynamics study of the dielectric properties of aqueous solutions of alanine and alanine dipeptide," *J. Chem. Phys.* **120**, 3333–15 (2004).
- ³⁵C. Schröder, J. Hunger, A. Stoppa, R. Buchner, and O. Steinhauser, "On the collective network of ionic liquid/water mixtures. II. Decomposition and interpretation of dielectric spectra," *J. Chem. Phys.* **129**, 184501–10 (2008).
- ³⁶D. Ben-Yaakov, D. Andelman, and R. Podgornik, "Dielectric decrement as a source of ion-specific effects," *J. Chem. Phys.* **134**, 074705 (2011).
- ³⁷M. Heyden, D. J. Tobias, and D. V. Matyushov, "Terahertz absorption of dilute aqueous solutions," *J. Chem. Phys.* **137**, 235103–9 (2012).
- ³⁸M. Sega, S. Kantorovich, and A. Arnold, "Kinetic dielectric decrement revisited: phenomenology of finite ion concentrations," *Phys. Chem. Chem. Phys.* **17**, 130–133 (2014).
- ³⁹M. Sega, S. S. Kantorovich, C. Holm, and A. Arnold, "Communication: Kinetic and pairing contributions in the dielectric spectra of electrolyte solutions," *J. Chem. Phys.* **140**, 211101–5 (2014).
- ⁴⁰K. F. Rinne, S. Gekle, and R. R. Netz, "Dissecting ion-specific dielectric spectra of sodium-halide solutions into solvation water and ionic contributions," *J. Chem. Phys.* **141**, 214502 (2014).
- ⁴¹K. F. Rinne, S. Gekle, and R. R. Netz, "Ion-Specific Solvation Water Dynamics: Single Water versus Collective Water Effects," *J. Phys. Chem. A* **118**, 11667–11677 (2014).
- ⁴²F. Fahrenberger, O. A. Hickey, J. Smiatek, and C. Holm, "The influence of charged-induced variations in the local permittivity on the static and dynamic properties of polyelectrolyte solutions," *J. Chem. Phys.* **143**, 243140–13 (2015).
- ⁴³M. Śmiechowski, J. Sun, H. Forbert, and D. Marx, "Solvation shell resolved THz spectra of simple aqua ions - distinct distance- and frequency-dependent contributions of solvation shells." *Phys. Chem. Chem. Phys.* **17**, 8323–8329 (2015).
- ⁴⁴C. Schaaf and S. Gekle, "Dielectric response of the water hydration layer around spherical solutes," *Phys. Rev. E* **92**, 032718 (2015).
- ⁴⁵U. Heugen, G. Schwaab, E. Bründermann, M. Heyden, X. Yu, D. M. Leitner, and M. Havenith, "Solute-induced retardation of water dynamics probed directly by terahertz spectroscopy," *Proc. Nat. Acad. Sci. (USA)*, 1–6 (2006).
- ⁴⁶H. Cui, B. Zhou, L.-S. Long, Y. Okano, H. Kobayashi, and A. Kobayashi, "A Porous Coordination-Polymer Crystal Containing One-Dimensional Water Chains Exhibits Guest-Induced Lattice Distortion and a Dielectric Anomaly," *Angew. Chem. Int. Ed.* **47**, 3376–3380 (2008).
- ⁴⁷R. Buchner and G. Hefter, "Interactions and dynamics in electrolyte solutions by dielectric spectroscopy," *Phys. Chem. Chem. Phys.* **11**, 8984 (2009).
- ⁴⁸K. J. Tielrooij, D. Paparo, L. Piatkowski, H. J. Bakker, and M. Bonn, "Dielectric Relaxation Dynamics of Water in Model Membranes Probed by Terahertz Spectroscopy," *Biophys J* **97**, 2484–2492 (2009).
- ⁴⁹K.-J. Tielrooij, J. Hunger, R. Buchner, M. Bonn, and H. J. Bakker, "Influence of Concentration and Temperature on the Dynamics of Water in the Hydrophobic Hydration Shell of Tetramethylurea," *J. Am. Chem. Soc.* **132**, 15671–15678 (2010).
- ⁵⁰U. Kaatzte, "Bound Water: Evidence from and Implications for the Dielectric Properties of Aqueous Solutions," *J. Mol. Liq.* **162**, 105–112 (2011).
- ⁵¹B. Zhou, A. Kobayashi, H.-B. Cui, L.-S. Long, H. Fujimori, and H. Kobayashi, "Anomalous Dielectric Behavior and Thermal Motion of Water Molecules Confined in Channels of Porous Coordination Polymer Crystals," *J. Am. Chem. Soc.* **133**, 5736–5739 (2011).
- ⁵²I. Rodríguez-Arteche, S. Cervený, Á. Alegría, and J. Colmenero, "Dielectric spectroscopy in the GHz region on fully hydrated zwitterionic amino acids," *Phys. Chem. Chem. Phys.* **14**, 11352–11 (2012).
- ⁵³D.-H. Choi, H. Son, S. Jung, J. Park, W.-Y. Park, O. S. Kwon, and G.-S. Park, "Dielectric relaxation change of water upon phase transition of a lipid bilayer probed by terahertz time domain spectroscopy," *J. Chem. Phys.* **137**, 175101 (2012).
- ⁵⁴X.-X. Zhang, M. Liang, J. Hunger, R. Buchner, and M. Maroncelli, "Dielectric Relaxation and Solvation Dynamics in a Prototypical Ionic Liquid + Dipolar Protic Liquid Mixture: 1-Butyl-3-Methylimidazolium Tetrafluoroborate + Water," *J. Phys. Chem. B* **117**, 15356–15368 (2013).
- ⁵⁵J. Sun, G. Niehues, H. Forbert, D. Decka, G. Schwaab, D. Marx, and M. Havenith, "Understanding THz Spectra of Aqueous Solutions: Glycine in Light and Heavy Water," *J. Am. Chem. Soc.* **136**, 5031–5038 (2014).
- ⁵⁶K. Mazur, R. Buchner, M. Bonn, and J. Hunger, "Hydration of Sodium Alginate in Aqueous Solution," *Macromolecules* **47**, 771–776 (2014).
- ⁵⁷S. Senapati and A. Chandra, "Dielectric Constant of Water Confined in a Nanocavity," *J. Phys. Chem. B* **105**, 5106–5109 (2001).
- ⁵⁸R. Blaak and J.-P. Hansen, "Dielectric response of a polar liquid trapped in a spherical nanocavity," *J. Chem. Phys.* **124**, 144714 (2006).
- ⁵⁹V. Ballenegger and J. P. Hansen, "Dielectric permittivity profiles of confined polar fluids," *J. Chem. Phys.* **122**, 114711 (2005).
- ⁶⁰W. Qi and H. Zhao, "Hydrogen bond network in the hydration layer of the water confined in nanotubes increasing the dielectric constant parallel along the nanotube axis." *J. Chem. Phys.* **143**, 114708 (2015).
- ⁶¹R. Renou, A. Szymczyk, G. Maurin, P. Malfreyt, and A. Ghoufi, "Superpermittivity of nanoconfined water," *J. Chem. Phys.* **142**, 184706–5 (2015).
- ⁶²Y. Lin, J. Shiomi, S. Maruyama, and G. Amberg, "Dielectric relaxation of water inside a single-walled carbon nanotube," *Phys. Rev. B* **80**, 045419–7 (2009).
- ⁶³H. Zhu, A. Ghoufi, A. Szymczyk, B. Balanec, and D. Morineau, "Anomalous Dielectric Behavior of Nanoconfined Electrolytic Solutions," *Phys. Rev. Lett.* **109**, 107801 (2012).
- ⁶⁴A. Ghoufi, A. Szymczyk, R. Renou, and M. Ding, "Calculation of local dielectric permittivity of confined liquids from spatial dipolar correlations," *Europhys. Lett.* **99**, 37008 (2012).

- ⁶⁵S. Gekle and A. Arnold, “Comment on “Anomalous Dielectric Behavior of Nanoconfined Electrolytic Solutions”,” *Phys. Rev. Lett.* **111**, 089801 (2013).
- ⁶⁶W. Qi, J. Chen, J. Yang, X. Lei, B. Song, and H. Fang, “Anisotropic Dielectric Relaxation of the Water Confined in Nanotubes for Terahertz Spectroscopy Studied by Molecular Dynamics Simulations,” *J. Phys. Chem. B* **117**, 7967–7971 (2013).
- ⁶⁷R. Renou, A. Szymczyk, and A. Ghoufi, “Tunable dielectric constant of water at the nanoscale,” *Phys. Rev. E* **91**, 032411–6 (2015).
- ⁶⁸M. J. Abraham, T. Murtola, R. Schulz, S. Páll, J. C. Smith, B. Hess, and E. Lindahl, “GROMACS: High performance molecular simulations through multi-level parallelism from laptops to supercomputers,” *SoftwareX* **1-2**, 19–25 (2015).
- ⁶⁹H. J. C. Berendsen, J. R. Grigera, and T. P. Straatsma, “The missing term in effective pair potentials,” *Journal of Physical Chemistry* **91**, 6269 (1987).
- ⁷⁰A. A. Kornyshev and M. A. Vorotyntsev, “Nonlocal Electrostatic Approach to the Double-Layer and Adsorption at the Electrode-Electrolyte Interface,” *Surface Science* **101**, 23–48 (1980).
- ⁷¹P. A. Bopp, A. A. Kornyshev, and G. Sutmann, “Static nonlocal dielectric function of liquid water,” *Phys. Rev. Lett.* , 1–4 (1996).
- ⁷²P. A. Bopp, A. A. Kornyshev, and G. Sutmann, “Frequency and wave-vector dependent dielectric function of water: Collective modes and relaxation spectra,” *J. Chem. Phys.* , 1–20 (1998).
- ⁷³A. A. Kornyshev, A. I. Rubinshtein, and M. A. Vorotyntsev, “Model nonlocal electrostatics: I,” *Journal of Physics C Solid State Physics* **11**, 3307 (1978).
- ⁷⁴A. A. Kornyshev and M. A. Vorotyntsev, “Model non-local electrostatics. III. Cylindrical interface,” *J Phys Chem* **12**, 4939–4946 (1979).
- ⁷⁵I. N. Bronstein and K. A. Semendjajew, *Handbook of Mathematics* (Springer, 1985).
- ⁷⁶M. V. Basilevsky and D. F. Parsons, “An advanced continuum medium model for treating solvation effects: Nonlocal electrostatics with a cavity,” *J. Chem. Phys.* **105**, 3734 (1996).
- ⁷⁷D. van der Spoel, P. J. van Maaren, and H. J. C. Berendsen, “A systematic study of water models for molecular simulation: Derivation of water models optimized for use with a reaction field,” *J. Chem. Phys.* **108**, 10220 (1998).